Computerized segmentation and measurement of malignant pleural mesothelioma

William F. Sensakovic,[a] Samuel G. Armato III, Christopher Straus, Rachael Y. Roberts, Philip Caligiuri, Adam Starkey, and Hedy L. Kindler
Department of Radiology, The University of Chicago, 5841 South Maryland Avenue, Chicago, Illinois 60637

(Received 13 August 2010; revised 12 November 2010; accepted for publication 16 November 2010; published 20 December 2010)

Purpose: The current linear method to track tumor progression and evaluate treatment efficacy is insufficient for malignant pleural mesothelioma (MPM). A volumetric method for tumor measurement could improve the evaluation of novel treatments, but a fully manual implementation of volume measurement is too tedious and time-consuming. This manuscript presents a computerized method for the three-dimensional segmentation and volumetric analysis of MPM.
Methods: The computerized MPM segmentation method segments the lung parenchyma and hemithoracic cavities to define the pleural space. Nonlinear diffusion and a k-means classifier are then implemented to identify MPM in the pleural space. A database of 31 computed tomography scans from 31 patients with pathologically confirmed MPM was retrospectively collected. Three observers independently outlined five randomly selected sections in each scan. The Jaccard similarity coefficient (J) between each of the observers and between the observer-defined and computer-defined segmentations was calculated. The computer-defined and the observer-defined segmentation areas (averaged over all observers) were both calculated for each axial section and compared using Bland–Altman plots.
Results: The median J value among observers averaged over all sections was 0.517. The median J between the computer-defined and manual segmentations was 0.484. The difference between these values was not statistically significant. The area delineated by the computerized method demonstrated variability and bias comparable to the tumor area calculated from manual delineations.
Conclusions: A computerized method for segmentation and measurement of MPM was developed. This method requires minimal initialization by the user and demonstrated good agreement with manually drawn outlines and area measurements. This method will allow volumetric tracking of tumor progression and may improve the evaluation of novel MPM treatments. [DOI: 10.1118/1.3525836]

Key words: image processing, computer-aided detection (CAD), segmentation, quantitative imaging, computed tomography (CT), malignant pleural mesothelioma (MPM)

I. INTRODUCTION

Malignant pleural mesothelioma (MPM) is a diffuse thickening of the visceral and/or parietal pleura that is primarily associated with asbestos exposure (Fig. 1). Although the yearly incidence of MPM in the United States may have already peaked due to the discontinuation of asbestos use as a building material, incidence in many countries is still rising.[1,2] Further, radiation therapy has recently been demonstrated as potential cause of MPM.[3,4] A diagnosis of MPM is associated with a median survival time from diagnosis of only 9–14 months.[5] This poor prognosis highlights the need for new treatment strategies and methods to accurately evaluate treatment efficacy.

The assessment of treatment efficacy or MPM progression relies on the measurement of tumor bulk (i.e., extent) on serial computed tomography (CT) scans. The ideal method to accurately measure tumor bulk requires three-dimensional (3D) delineation of disease and volume calculation on each CT scan. Progression or response to therapy is then determined by subtracting the volumes calculated from the same patient at two serial time points. Manual 3D delineation of tumor is practical only when the tumor extent is small and the morphology is compact (as it is for lung nodules); however, MPM grows circumferentially around the lung (Fig. 1) and may span more than 100 CT sections (assuming a section thickness of 1 mm). This large number of sections makes manual delineation too tedious and time-consuming to be implemented in either clinical or research settings. The current standard (Fig. 2) for determining MPM tumor bulk is defined by the modified response evaluation criteria in solid tumors (RECIST).[6] This manual method does not delineate the diseased volume, but instead utilizes two one-dimensional (1D) tumor thickness measurements obtained from three axial sections in each CT scan of the patient. These six linear measurements are then summed to compute a number that is meant to represent of tumor bulk and the tumor bulk measurements obtained from serial scans are compared to estimate MPM progression or response to therapy. The modified RECIST protocol was designed to be fast and easy to implement; however, several studies have identified sources of variability and error in the implementation of the modified RECIST protocol,[7] including variability

FIG. 1. Unilateral MPM presenting in the left hemithorax (black arrows).

due to observer selection of corresponding serial sections[8] or measurement sites[9] and nonuniform tumor growth. Studies have also demonstrated a low concordance rate for linear and area tumor burden measurements[10] and high variability in area-based growth assessment for diseases classified as stable by linear measurements.[11]

The caseloads to which clinicians and radiologists are subject and the increasingly larger image data sets acquired during a typical thoracic CT scan make manual segmentation and volumetric measurement of MPM unrealistic. As an example, consider a MPM tumor that spans 150 CT sections. If an observer averages 20 s per section to delineate tumor, then 50 min per case would be required to perform a complete manual delineation of tumor volume (segmentations acquired during the course of our research actually required 1.5 h). In the research setting, a database of 50 patient scans would require 42 work hours per observer. The high time-cost, tedious nature of manual delineation, and many sources of error and variability, coupled with a study that correlates tumor volume and median survival time for mesothelioma patients,[12] imply that the next step for assessment of mesothelioma tumor burden, disease progression, and treatment efficacy should be computerized volumetric measurement. Three-dimensional segmentation of disease may also provide useful information for presurgical staging and identification of patients suitable for surgical intervention by providing positional and size information.[12,13] This study introduces a computerized method for the segmentation (delineation) and volumetric measurement of MPM on thoracic CT scans. The computerized method is validated against two-dimensional (2D) manual delineations of MPM.

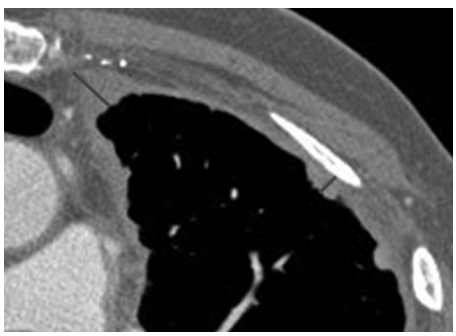

FIG. 2. Example of modified response evaluation criteria in solid tumors (RECIST) measurements (dark gray lines) for MPM.

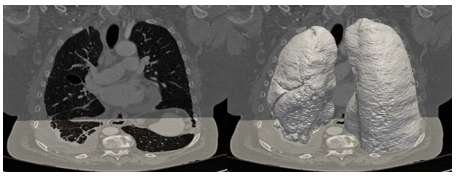

FIG. 3. Example of lung segmentation. Note that tumor is excluded from the lung segmentation in the right hemithorax.

II. MATERIALS AND METHODS

The computerized MPM segmentation method[14] is composed of three major steps: (1) Segmentation of lung parenchyma, (2) segmentation of hemithoracic cavity, and (3) segmentation and measurement of MPM. The focus of this paper is the specific segmentation of MPM; thus, only an overview of steps 1 and 2 will be given here.

II.A. Lung segmentation

The segmentation of lung parenchyma is a fully automated method based on gray level, texture, and shape analysis. The lung parenchyma segmentation algorithm begins by processing the scan axially on a section-by-section basis. First, the thorax is segmented from the surrounding nonanatomic structures such as the CT table and blankets. The airway (trachea and bronchi) is then identified and removed from the thoracic segmentation. An intensity threshold of −200 Hounsfield units (HU) is applied to the thoracic segmentation with the airway removed and all pixels below this threshold are retained to create an image of lung parenchyma candidate regions. Several refinements are then applied to each candidate region to eliminate false-positive candidates and improve segmentation quality. All 2D candidate regions with an area less than 1 cm^2 or with an extent less than 3 pixels in any dimension are eliminated. A concavity elimination algorithm[15] is applied to the medial surface of each 3D candidate to ensure that the major vessels of the lungs are included in the final segmentation while excluding disease. Finally, a modified directional gradient correlation filter[16] is applied to remove 3D candidate regions that are actually air-filled bowel. All remaining candidate regions are identified as lung parenchyma (Fig. 3). A small in-house pilot review of the lung parenchyma segmentation algorithm found an average J of 0.949 ± 0.046.

II.B. Hemithoracic cavity segmentation

The hemithoracic cavities are the 3D volumes that lung parenchyma would occupy in the absence of disease. Because both the visceral pleura and parietal pleura are normally invisible on CT scans, alternate bounding structures must be identified to define the hemithoracic cavities. The medial surface of a hemithoracic cavity is defined by the vertebral bodies and the mediastinum, which includes fat,

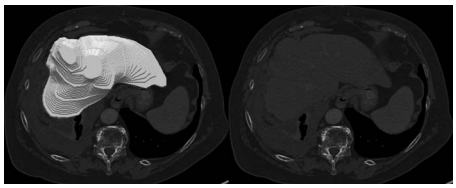

FIG. 4. Example of liver segmentation.

connective tissue, the heart, great vessels, and airway. The superior, anterior, posterior, and lateral surfaces of a hemithoracic cavity are bound by the ribs and vertebral bodies. The inferior surface is bound by the diaphragm, which is not visible on CT images, and thus the liver and spleen are used to visually define the inferior boundary of the right and left hemithoracic cavities, respectively. The ribs, vertebrae, and structures exhibiting high intensities due to contrast media uptake (e.g., heart, aorta, spleen, and vessels of the lungs and liver) are segmented from the surrounding tissue by retaining pixels within the thoracic boundary with values greater than the empirically defined threshold of 150 HU. A series of morphological operators is then applied to eliminate noise and fill "holes" in this bone/contrast segmentation.

The bone/contrast segmentation partially defines the superior, anterior, posterior, lateral, and medial surfaces of the hemithoracic cavities. The bone/contrast segmentation may also partially define the inferior boundary of the hemithoracic cavity if the spleen and/or liver are sufficiently enhanced by the contrast media. Unfortunately, liver parenchyma (especially the superior surface which bounds the hemithoracic cavities) does not usually exhibit sufficient contrast media uptake to be accurately segmented by the bone/contrast segmentation method. The similar densities of liver parenchyma and MPM make the accurate segmentation of the liver based on HU difficult and thus a semiautomated method is implemented.

The semiautomated liver segmentation method (Fig. 4) requires the observer to delineate the approximate liver boundary in several axial CT sections. The user is not required to completely segment the liver, but only a portion of the superior surface of the liver that acts as a boundary for the hemithoracic cavity. Typically, if the superior portion of the liver spans 70 axial sections, 10 axial sections require manual outlining of the liver (assuming 1 mm section thickness). The sections are chosen by the user with the constraint that the superiormost axial section containing the liver must be outlined and that any section where the 2D topology of the liver changes (i.e., there is a separation or merging of liver regions in adjacent axial sections) should also be outlined. The segmentation method then applies shape-based interpolation[17,18] to the user-defined outlines to create a 3D segmentation of the superior surface of the liver. The observer time-cost for semiautomated liver segmentation (the only observer interaction necessary in the computerized method) was 106.8 ± 32.7 s, where the variation in time depended on liver/lung parenchyma morphology and liver/MPM contrast.

The liver and spleen segmentations bound a small portion of the inferior surface of the hemithoracic cavities; thus, fat is included as a bounding structure to fill some of the "gaps" between the actual hemithoracic cavity surface and the liver/spleen segmentations. Fat segmentation proceeds by smoothing all axial sections using nonlinear diffusion[19] and retaining all pixels in the range of [−190 HU, −30 HU].[20]

Fat segmentation improves the definition of the hemithoracic cavity inferior boundary and improves the definition of the mediastinal boundary by filling some (though not all) gaps between the mediastinal structures. The fat, liver, and bone/contrast segmentations partially define the 3D boundary of each hemithoracic cavity; however, segmentation of the hemithoracic cavities requires the interpolation of the bounding structure surfaces into continuous 3D surfaces. A geometric level-set active surface method[21] is implemented for this purpose. The surface is initialized as the surface of the lung parenchyma and the final position of the active surface is identified as the boundary of the hemithoracic cavity. A small in-house pilot review of the hemithoracic cavity segmentation found an average J of 0.920 ± 0.065.

II.C. MPM segmentation and measurement

Once the hemithoracic cavities are identified, the third step begins by asking the observer to indicate whether the disease is present in the right, left, or both hemithoracic cavities. If the disease is unilateral, analysis proceeds only on the hemithorax containing disease. Separation of the MPM tumor from normal anatomy begins by identifying the pleural space. The pleural space is the 3D region located between the visceral and parietal pleurae. When disease (e.g., MPM) infiltrates the pleural space, the lung parenchyma is deformed and the pleural space is visible on CT scans as the region between the lung parenchyma and hemithoracic cavity boundary. Specifically, the pleural space segmentation is created according to $PS = HTC \cap (LP)^C$, where $(\ )^C$ indicates the complement of the set, PS is the pleural space segmentation, HTC is the hemithoracic cavity segmentation, and LP is the lung parenchyma segmentation. A 5×5 pixel morphological opening operator[22] is then applied to the pleural space segmentation to eliminate errors arising from imprecision in the hemithoracic cavity and lung parenchyma segmentations.

The remaining pixels, which constitute the pleural space, are then set to the HU of a nonlinear diffusion smoothed image of the patient. Nonlinear diffusion smoothing is a generalization of Gaussian smoothing based on a differential equation of the porous medium type.[23,24] The purpose of nonlinear diffusion smoothing is to retain and localize image edges while smoothing image regions with similar intensities. Nonlinear diffusion smoothing is an intensive, iterative technique and is applied on a section-by-section basis to axial CT sections (rather than volumetrically) to reduce both computation time and system memory requirements. Nonlinear diffusion is implemented for 40 iterations with the diffusitivity (d) equation

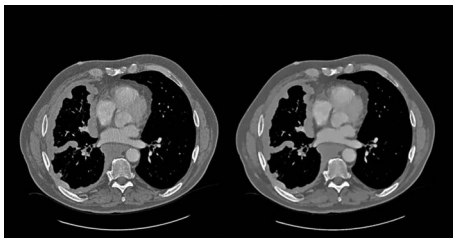

FIG. 5. Left: Axial CT section with MPM in the right hemithorax. Right: Nonlinear diffusion smoothed CT section.

$$d = \begin{matrix} 1, & (s \le 0) \\ 1 - \exp(-C\lambda^{10}/s^{10}), & (s > 0) \end{matrix},$$

where λ is 3 for the first 30 iterations and increases linearly from 3 to 10 for the final ten iterations, s is the edge value of a derivative of Gaussian filter[22] applied to the CT section with σ (i.e., the standard deviation of the Gaussian) of 3 for the first 30 iterations and decreasing linearly from 1.0 to 0.1 for the final 10 iterations, and C is a constant derived to satisfy the equations (Fig. 5)

$$\begin{matrix} s * d(s) > 0 & \text{for} & s < \lambda \\ s * d(s) < 0 & \text{for} & s > \lambda \end{matrix}.$$

MPM presents on CT scans with intensity values roughly in the range of [0 HU, 100 HU]. A 1D k-means classifier[22] is applied to the pleural space segmentation of the affected hemithorax. The k-means classifier applied in this algorithm groups the pixels of the pleural space segmentation into nine categories based on the difference between the pixel HU and the average HU of each category. The average HU of each category is then recalculated and the pixels are reclassified. This category HU update and reclassification repeats until the category HU update produces no changes in classification. The categories are initialized with mean HU values of −10 000 (extrapleural space), −500 (air/lung), −200 (air/lung/fat), −50 (fat/soft tissue), 0 (soft tissue/mesothelioma/effusion), 50 (soft tissue/mesothelioma/effusion), 100 (soft tissue/mesothelioma/cartilage), 200 (mesothelioma/cartilage/bone), and 500 HU (bone/metal/contrast media). All pixels in the first two or last categories are eliminated from the segmentation. The remaining pixels of the pleural space are identified as MPM (Fig. 6). Finally, it should be noted that this computerized method utilizes several parameters (e.g., initial k-means categories) that could impact segmentation performance. All parameters used in this study were determines empirically on a database of images that was separate from the testing database.

II.D. Testing methodology

A database of 31 scans from 31 patients (26 males and 5 females; age range: 50–83 yr; mean: 68 ± 10 yr) with pathologically confirmed MPM was retrospectively collected. Each scan was reconstructed axially as a series of 512 × 512-pixel images by either a Philips (Philips Medical Systems, Cleveland, OH) Brilliance 16 (n=23), Brilliance 40 (n=1), or Brilliance 64 (n=7) scanner with a mean in-plane pixel spacing of 0.725 ± 0.084 mm/pixel and a mean slice thickness of 1.023 ± 0.805 mm/pixel.

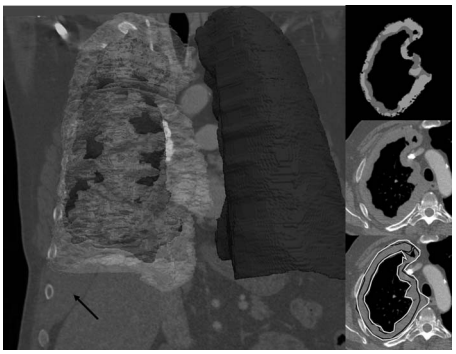

FIG. 6. CT scan of a patient with mesothelioma. Left: Lung parenchyma segmentation (dark gray) and mesothelioma segmentation (transparent white) are superimposed. Note that a portion of mesothelioma was incorrectly excluded from the segmentation (black arrow). Right top: Axial cross-section of mesothelioma segmentation. Each gray level represents a different class created by the k-means classifier. Right middle: Axial cross-section of original CT scan. Right bottom: Axial CT cross-section with observer segmentations superimposed: Observer A (white), observer B (black), and observer C (dark gray).

Three observers (two attending radiologists and one resident) independently outlined 5 sections in each of the 31 patient scans. Sections for analysis were selected randomly by a computer algorithm subject to the criteria that sections selected in the same patient were separated by 1 cm when possible to reduce anatomic correlation between sections. Outlines were performed using Abras, an in-house computerized system for visualization and annotation. This system allowed for user-controlled window/level and zoom. All sections in each scan were visible to the observer to aid in analysis. Outlines were created by placing vertices along the boundary of the tumor using the mouse and these vertices were connected with straight lines to form an outline of the tumor. Further, observers could add, delete, or move vertices to refine an outline. Observers were not restricted to using a specified computer terminal. Scans demonstrating prominent calcifications (n=6) or surgical intervention (n=2) were excluded from further analysis, resulting in a total of 23 scans for testing. The Jaccard similarity coefficient (J) between each of the observers was calculated as: $J = \text{Area}(OS_1 \cap OS_2)/\text{Area}(OS_1 \cup OS_2)$; where Area() is the area of the set, OS_1 is the segmentation defined by one observer, and OS_2 is the segmentation defined by a different observer. This metric creates a single number between 0 (no overlap between segmentations) and 1 (identical segmentations).

Observer segmentation of MPM in CT scans is a difficult task that may exhibit large interobserver variability. CT sections where the observers disagree about the boundary position or even the existence of tumor are not suitable to use as "truth" for validating automated methods. The mean J value over all observers for each section was used as a metric to determine which sections demonstrated disease that was regularly identified by the observers and thus suitable for use

as truth. Sections where the mean J value was less than or equal to 0.333 or where no disease was present on the axial section were excluded from further analysis. The value 0.333 (chosen prior to beginning the experiment) corresponds to the J that would be calculated if two square regions overlapped by half.

The computerized method was applied to all remaining sections (n=66). Liver segmentation initializations for the computerized method were created by a single observer (W.F.S.) who did not provide manual mesothelioma segmentations (i.e., truth). The computer-defined segmentation accuracy was evaluated by determining the J between each of the observer-defined mesothelioma segmentations and the computer-defined mesothelioma segmentations on the corresponding section. The Jaccard similarity coefficient here is define as $J = \text{Area}(OS \cap CS)/\text{Area}(OS \cup CS)$ where Area() is the area of the set, OS is an observer-defined (manual) segmentation, and CS is the computer-defined segmentation. Significance was tested for J values calculated between the computer-defined and manual segmentations and J values calculated between pairs of manual segmentations using a one-sided Wilcoxon signed-rank test ($\alpha=0.1$).

The ultimate goal of the computerized method is the accurate assessment of tumor extent using volume derived from the computerized segmentations. In this study, the areas of the manual and computerized outlines are used to assess the accuracy of tumor extent measurements derived from computerized segmentations. The computer-defined segmentation area and observer-defined segmentation area (averaged over all observers) were both calculated for each axial section and compared using Bland–Altman plots. The areas of the observers with the highest and lowest average J calculated between their segmentations were also compared using Bland–Altman plots.

III. RESULTS

The average J values between observers averaged over all sections was 0.480 ± 0.151 (median: 0.476), 0.466 ± 0.158 (median: 0.455), and 0.650 ± 0.153 (median: 0.686) for observers A/B, B/C, and A/C, respectively. A total of 66 sections from 19 patients were used to validate the automated system. The average J between the computer-defined and manual segmentations was 0.506 ± 0.218 (median: 0.539), 0.407 ± 0.194 (median: 0.430), and 0.493 ± 0.223 (median: 0.514) for observers A, B, and C, respectively. An example of the computer-defined segmentation is given in Fig. 6. J values calculated between the computer-defined and manual segmentations did not demonstrate a statistically significant difference from J values calculated between pairs of manual segmentations using a one-sided Wilcoxon signed-rank test (p=0.731). Statistical power calculated retrospectively for this comparison was 0.224. Eleven axial sections were excluded from analysis because the observers agreed that no disease was present in these sections. Three of the eleven sections (27.3%) were also correctly identified as containing no disease by the computerized segmentation method.

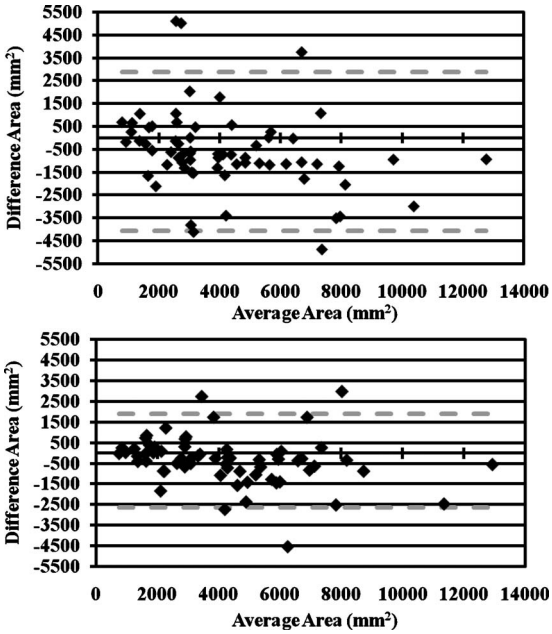

FIG. 7. Bland–Altman plots of mesothelioma area. Top: Comparison of computer-defined area and average area over all observers. Bottom: Comparison of manual area for observers with the highest average J (observers A and C). The gray dashed line indicates the 95% limits of agreement.

The Bland–Altman plot comparing the mean area over all observers for each section and the computer-defined area is given in Fig. 7. The mean area over all 66 patient sections was 3899.02 ± 2379.13 and 4492.21 ± 2879.36 mm^2 for manual and computer-defined segmentations, respectively. The mean difference over all patient sections was -593.19 ± 1768.44 mm^2 and the 95% limits of agreement for the differences were (−4059.34, 2872.96). The Bland–Altman plot comparing the areas defined by the observers with the highest average J value over all sections (observers A and C) is given in Fig. 7. The mean difference over all patient sections was -366.96 ± 1162.39 mm^2 and the 95% limits of agreement for the differences were (−2645.24, 1911.32). The Bland–Altman plot comparing the areas defined by the observers with the lowest average J value (observers B and C) demonstrated a mean difference over all patient sections of -909.52 ± 1819.85 mm^2 and 95% limits of agreement for the differences of (−2657.39, 4476.43).

IV. DISCUSSION

The automated segmentation of MPM is an extremely difficult biomedical image processing task. MPM is not distinguishable from the surrounding soft tissue based on either density (HU) or gradient information alone and has no distinguishable texture on CT scans. This makes simple segmentation methods such as thresholding, region growing, texture filtering, and active contours ineffective if applied directly for tumor segmentation. MPM grows nonuniformly and circumferentially around the lung and may consist of several separate 3D regions or a single region encasing the entire lung. Further, the tumor may grow in fingerlike projections along the fissures of the lung or hilar vessels and can

invade the chest wall, abdomen, or mediastinum (Fig. 1). This makes shape-based and morphology-based analysis difficult. Finally, the large extent and complex morphology of MPM make user-guided segmentation of the tumor difficult due to an inability to define a shape-invariant tumor model. Without a robust tumor model, a large number of user-defined control points are necessary to accurately delineate the tumor surface, making semiautomated segmentation too time-consuming in practice.

The complex nature of the segmentation task makes a more comprehensive approach to MPM segmentation necessary. Instead of attempting to directly segment the tumor, the computerized method presented in this study roughly delineates the pleural space based on other, more easily identified, anatomic landmarks. This rough delineation is used to restrict refinement methods to a subset of the original scan, thus reducing segmentation error.

Qualitatively, the largest computerized MPM segmentation errors tended to occur in the lung bases and intercostal spaces where segmentation of the hemithoracic cavities was most difficult. Other segmentation errors were related to the uneven distribution of contrast media, presence of concurrent disease (e.g., effusion), and partial volume effect creating pixels with HU values similar to mesothelioma.

Bland–Altman plots indicated that the computerized method overestimated the actual area (represented by the mean area of all observer segmentations) by 593 mm^2 on average. This value is larger than the bias of observer A compared to observer C (366 mm^2), but is smaller than that of observer B compared to observer C (910 mm^2). The large bias demonstrated by the computerized segmentation method is due to leakage of the active surface used in the hemithoracic cavity segmentation method and could be improved by either manual refinement or restricting the hemithoracic cavity to the axial convex hull of the bone/contrast segmentation. The variance in area differences did not demonstrate a strong trend as a function of mean tumor area for either the computerized or manual comparisons of area.

The major limitation of this study was the testing database size. MPM is a rare disease with an incidence rate of only nine cases per million people[25] in the United States and a short survival time making the acquisition of a large database at a single institution difficult. In this study, five sections per patient were randomly selected for analysis under the condition that selected sections within the same patient were separated by 1 cm to reduce correlation between selected sections. Observer outlines were used as truth to validate the computerized method, so a condition that observers agree on the existence and position of MPM further reduced the testing database. The low retrospectively calculated statistical power was due to the small testing database ($n=66$ sections) and small difference between the computer and observer outlines (which was the goal of the computerized method). A testing database of $n=644$ sections would be necessary for statistically powerful ($1-\beta=0.8$) hypothesis testing of a difference in medians as demonstrated in this study. The computerized method will be implemented in future studies to help evaluate novel therapies and a future study could aggregate samples from several of these studies to re-evaluate the computerized method with a larger testing database. Analysis could also be improved by expanding the patient database so only a single section is drawn from each patient (thus ensuring no correlation exists between samples). Finally, validation of the computerized method was limited because 2D observer-created outlines were used instead of 3D observer-created volumes. The ideal validation method would be to compare 3D observer-created delineations with the 3D computer-generated delineations. Unfortunately, the tedious and time-consuming nature of manual MPM delineation (which also provides motivation for the creation of a computerized method) coupled with the large number of samples necessary for statistically powerful testing make the use of 3D observer outlines as truth unlikely even in future studies.

The ultimate goal of MPM segmentation is the localization and volumetric measurement of disease with minimal observer time-cost for incorporation into staging and prognostic disease models. The agreement between the computer-defined and manual segmentations and areas indicates that the computerized method effectively segments MPM for a range of scans. Further, the time-cost to the observer was reduced from hours to minutes. Segmentations created by the computerized method are not yet sufficient to directly incorporate into staging or prognostic disease models and will require further manual refinement to ensure accuracy (especially in the base of the lungs and in cases with concurrent disease).

Future work will incorporate the computerized method into Abras, our in-house measurement and visualization system, create specific tools to aid in the fast manual refinement of the mesothelioma segmentations, and apply the computerized method to evaluate MPM tumor extent and position as indicators of disease stage, patient prognosis, and treatment efficacy.

V. CONCLUSION

The set of methods developed in this study is expected to provide the radiologist with 3D positional and volumetric information that would otherwise be too tedious and time-consuming to acquire manually. We expect that the computerized methods developed in this manuscript will make the evaluation of pleural-based abnormalities both more consistent and efficient. These methods will allow a clinician to track pleural-based abnormalities over temporally sequential scans and measure changes in size. These changes will facilitate the objective assessment of treatment effectiveness for each patient. Further, estimates of disease progression and treatment efficacy will be more accurate because they will be based on changes in volume instead of linear measurements made on CT or size estimations based on radiographs. We anticipate that the use of volumetric measurements will provide useful information when making treatment decisions. Though it is beyond the scope of the current investigation, we hope that the addition of a "computer reader" will act to improve both the efficacy and effi-

ciency of observer interpretations. Further, we believe that these methods will be invaluable to researchers who attempt to create novel treatments for pleural-based diseases and require objective response data to evaluate these treatments.

ACKNOWLEDGMENTS

The authors would like to thank Neal Corson and Alexandra Cunliffe for their help testing the computerized segmentation method and Zacariah E. Labby for his assistance with statistical significance testing. This study was supported by USPHS Grant No. R01CA102085.

[a]Author to whom correspondence should be addressed. Electronic mail: wfsensak@uchicago.edu; Telephone: 773-834-107; Fax: 773-702-0371.

[1]R. H. Weill, J. Hughes, and A. Churg, "Changing trends in US mesothelioma incidence," Occup. Environ. Med. **61**, 438–441 (2004).
[2]J. Peto, A. Decarli, C. La Vecchia, F. Levi, and E. Negri, "The European mesothelioma epidemic," Br. J. Cancer **79**, 666–672 (1999).
[3]H. Yang, J. R. Testa, and M. Carbone, "Mesothelioma epidemiology, carcinogenesis, and pathogenesis," Curr. Treat. Options Oncol. **9**, 147–157 (2008).
[4]J. E. Goodman, M. A. Nascarella, and P. A. Valberg, "Ionizing radiation: A risk factor for mesothelioma," Cancer Causes Control **20**, 1237–1254 (2009).
[5]N. J. Vogelzang, J. J. Rusthoven, J. Symanowski, C. Denham, E. Kaukel, P. Ruffie, U. Gatzemeier, M. Boyer, S. Emri, C. Manegold, C. Niyikiza, and P. Paoletti, "Phase III study of pemetrexed in combination with cisplatin versus cisplatin alone in patients with malignant pleural mesothelioma," J. Clin. Oncol. **21**, 2636–2644 (2003).
[6]M. J. Byrne and A. K. Nowak, "Modified RECIST criteria for assessment of response in malignant pleural mesothelioma," Ann. Oncol. **15**, 257–260 (2004).
[7]S. G. Armato III, G. R. Oxnard, H. MacMahon, A. Starkey, N. J. Vogelzang, H. L. Kindler, and M. Kocherginsky, "Measurement of mesothelioma on thoracic CT scans: A comparison of manual and computer-assisted techniques," Med. Phys. **31**, 1105–1115 (2004).
[8]W. F. Sensakovic, S. G. Armato III, A. Starkey, and J. L. Ogarek, "Automated matching of temporally sequential CT sections," Med. Phys. **31**, 3417–3424 (2004).
[9]S. G. Armato III, J. L. Ogarek, A. Starkey, N. J. Vogelzang, H. L. Kindler, M. Kocherginsky, and H. MacMahon, "Variability in mesothelioma tumor response classification," AJR, Am. J. Roentgenol. **186**, 1000–1006 (2006).
[10]A. K. Nowak, S. G. Armato III, G. L. Ceresoli, H. Yildirim, and R. J. Francis, "Imaging in pleural mesothelioma: A review of imaging research presented at the 9th International Meeting of the International Mesothelioma Interest Group," Lung Cancer **70**, 1–6 (2010).
[11]S. G. Armato III, E. A. Pearson, R. Y. Roberts, W. F. Sensakovic, and P. Caligiuri, "Assessment of mesothelioma tumor response: Correlation of tumor thickness and tumor area," Med. Phys. **34**, 2554 (2007).
[12]H. I. Pass, B. K. Temeck, K. Kranda, S. M. Steinberg, and I. R. Feuerstein, "Preoperative tumor volume is associated with outcome in malignant pleural mesothelioma," J. Thorac. Cardiovasc. Surg. **115**, 310–318 (1998).
[13]R. Heelan, "Staging and response to therapy of malignant pleural mesothelioma," Lung Cancer **45**, S59–S61 (2004).
[14]W. F. Sensakovic, "Computerized segmentation and measurement of pleural disease," Ph.D. thesis, The University of Chicago, 2010. See http://www.medphys.org/PhDAbstracts/sensakovicphd.pdf.
[15]W. F. Sensakovic, S. G. Armato III, and A. Starkey, "A general method for the identification and repair of concavities in segmented medical images," in Proceedings of the IEEE NPSS/MIC, Dresden, Germany, October 2008 (unpublished).
[16]W. F. Sensakovic, A. Starkey, and S. G. Armato III, "A modified gradient correlation filter for image segmentation: Application to airway and bowel," Med. Phys. **36**, 480–485 (2009).
[17]G. T. Herman, Z. Jingsheng, and C. A. Bucholtz, "Shape-based interpolation," IEEE Comput. Graphics Appl. **12**, 69–79 (1992).
[18]S. P. Raya and J. K. Udupa, "Shape-based interpolation of multidimensional objects," IEEE Trans. Med. Imaging **9**, 32–42 (1990).
[19]J. Weickert *et al.*, "Parallel implementations of AOS schemes: A fast way of nonlinear diffusion filtering," in Proceedings of the 1997 IEEE International Conference on Image Processing, Vol. 3, pp. 396–399, 1997 (unpublished).
[20]Y. Tohru, N. Tadashi, Y. Mitsukazu, H. Abdul, M. Masakazu, Y. Kouichi, A. Takeshi, K. Kazuaki, F. Tohru, Y. Shizuya, and M. Yuji, "Abdominal fat: Standardized technique for measurement at CT," Radiology **211**, 283–286 (1999).
[21]L. Ibanez, W. Schroeder, L. Ng, and J. Cates, "The Insight Toolkit (ITK)." See www.itk.org, 2009.
[22]M. Šonka, V. Hlaváč, and R. Boyle, *Image Processing, Analysis, and Machine Vision*, 2nd ed. (PWS, Pacific Grove, 1999).
[23]J. Weickert, "Theoretical foundations of anisotropic diffusion in image processing," Computing Supplementum **11**, 221–236 (1996).
[24]F. Catté, P. L. Lions, J. M. Morel, and T. Coll, "Image selective smoothing and edge detection by nonlinear diffusion," SIAM (Soc. Ind. Appl. Math.) J. Numer. Anal. **29**, 182–193 (1992).
[25]C. Bianchi and T. Bianchi, "Malignant mesothelioma: Global incidence and relationship with asbestos," Ind. Health **45**, 379–387 (2007).